RSC Advances

PAPER

View Article Online
View Journal | View Issue

Cite this: *RSC Adv.*, 2026, **16**, 30676

Pharmacophore-targeted fluorescence sensing of ibrutinib *via* Michael addition-induced electron transfer on thiol-functionalized carbon dots

Mohamed N. Goda,[a] Laila S. Alqarni,[a] Faisal K. Algethami,[a] Hossieny Ibrahim,[bg] Mohamed M. El-Wekil,[cd] Ramadan Ali,[e] Suliman A. Almahmoud[f] and Al-Montaser Bellah H. Ali *[c]

Ibrutinib (IBR), an irreversible inhibitor of Bruton's tyrosine kinase, is commonly used as a first-line therapy for chronic lymphocytic leukemia (CLL) and various other B-cell cancers. Given its narrow therapeutic window and the clinical necessity of long-term administration, accurate therapeutic drug monitoring of IBR in biological fluids is of paramount importance. Herein, we report a novel fluorometric sensing platform for the selective and sensitive determination of IBR based on thiol-functionalized carbon dots (HS-CDs). The sensing mechanism relies on the specific covalent interaction between the –SH groups on HS-CDs and the electrophilic acrylamide moiety of IBR through a rapid Michael addition reaction, which anchors IBR to the CD surface. This binding modifies the local electronic environment of the carbon dots and promotes efficient electron interaction between the electron-rich nitrogen-containing groups of IBR and the CD fluorophore, collectively leading to a concentration-dependent enhancement of fluorescence. The sensor, under optimized conditions, responded linearly from 1.0 to 30.0 ng mL^{-1}, with a minimum detectable concentration of 0.21 ng mL^{-1}. The practical applicability of the platform was demonstrated through the direct quantification of IBR in human serum samples collected from CLL patients, achieving satisfactory recovery values (97.0–100.2%) with minimal sample preparation. The proposed method has strong potential for routine therapeutic drug monitoring in CLL patients undergoing ibrutinib therapy.

Received 7th April 2026
Accepted 16th May 2026

DOI: 10.1039/d6ra02905a

rsc.li/rsc-advances

1. Introduction

Ibrutinib (IBR) is a BTK inhibitor that irreversibly targets Bruton's tyrosine kinase and is clinically approved to treat B-cell malignancies like chronic lymphocytic leukemia, Waldenström's macroglobulinemia, and mantle cell lymphoma.[1,2] Its mechanism involves permanent covalent binding to cysteine-481 in the BTK active site, thereby blocking B-cell receptor signaling pathways that drive malignant cell growth and survival. Following oral administration (420–560 mg per day), IBR reaches peak plasma concentrations within 1–2 hours, with plasma levels ranging from 10 to 500 ng mL^{-1} and a half-life of 4–6 hours; urine and saliva concentrations are also documented at variable levels.[3,4] Despite its efficacy, IBR carries significant adverse effects including atrial fibrillation, bleeding complications, hypertension, and opportunistic infections.[5] Considerable interpatient pharmacokinetic variability—driven by CYP3A4 polymorphisms, drug interactions, and food effects—means that subtherapeutic levels risk disease progression while supratherapeutic exposure increases hemorrhagic and cardiovascular toxicity.[6,7] Therapeutic drug monitoring (TDM) is therefore clinically essential for dose individualization, toxicity prevention, and adherence assessment.

Existing analytical methods for IBR quantification each carry significant limitations that collectively hinder their routine clinical implementation. HPLC-MS/MS represents the current reference standard, offering exceptional sensitivity and specificity; however, its reliance on costly triple-quadrupole instrumentation, labor-intensive sample pretreatment involving protein precipitation or solid-phase extraction, and the requirement for highly trained personnel render it largely incompatible with high-throughput therapeutic drug monitoring in routine clinical settings.[8–10] HPLC-UV/PDA methods offer a more accessible and affordable alternative, yet they

[a]*Department of Chemistry, College of Science, Imam Mohammad Ibn Saud Islamic University (IMSIU), Riyadh 11623, Saudi Arabia*
[b]*School of Biotechnology, Badr University in Assiut (BUA), Assiut, Egypt*
[c]*Department of Pharmaceutical Analytical Chemistry, Faculty of Pharmacy, Assiut University, Assiut, Egypt. E-mail: Almontaser_bellah@aun.edu.eg*
[d]*Pharmaceutical Chemistry Department, Faculty of Pharmacy, Badr University in Assiut (BUA), Assiut, 2014101, Egypt*
[e]*Department of Pharmaceutical Chemistry, Faculty of Pharmacy, University of Tabuk, Tabuk 71491, Saudi Arabia*
[f]*Department of Medicinal Chemistry and Pharmacognosy, College of Pharmacy, Qassim University, Buraydah 51452, Saudi Arabia*
[g]*Department of Chemistry, Faculty of Science, Assiut University, Assiut 71516, Egypt*

frequently deliver inadequate sensitivity, with reported LOD values often insufficient for accurate monitoring of IBR trough concentrations—which can fall in the low ng mL^{-1} range—and their selectivity is easily compromised in complex biological matrices such as plasma and serum.[11] Electrochemical approaches, including differential pulse voltammetry and square wave voltammetry, present attractive cost-effectiveness and miniaturization potential; however, they are significantly hampered by progressive electrode fouling in protein-rich biological fluids, susceptibility to interference from electroactive endogenous species such as ascorbic acid and uric acid, and the frequent observation of narrow linear dynamic ranges that limit their practical utility for clinical IBR quantification.[12,13] Immunoassay-based platforms, despite their widespread use in TDM of other oncology drugs, remain unavailable for IBR, primarily because the structural complexity of its scaffold and the reactive acrylamide warhead present considerable challenges in generating antibodies with the required affinity and selectivity. Spectrophotometric methods, while instrumentally straightforward and widely available, generally lack the selectivity required for direct analysis in biological fluids and are susceptible to inner filter effects, background matrix absorption, and in some cases dependence on organic solvents or derivatization reagents that complicate sample handling.[14] Taken together, these limitations underscore the urgent need for a simple, sensitive, selective, and matrix-compatible analytical platform capable of supporting reliable IBR monitoring in clinical practice.

Functionalized carbon dots (CDs) have emerged as highly versatile fluorescent nanomaterials for pharmaceutical analysis in biological fluids, owing to their exceptional photostability, tunable emission, low cytotoxicity, aqueous dispersibility, and the ease with which their surfaces can be tailored with selective recognition elements.[15,16] Surface functionalization with specific functional groups, molecularly imprinted polymers (MIPs),[17,18] aptamers, or metal ion complexes enables CDs to interact selectively with target drug molecules through hydrogen bonding, electrostatic interactions, π–π stacking, or coordination chemistry, producing concentration-dependent fluorescence (FL) quenching or enhancement responses.[19,20] This approach has been successfully applied to the detection of numerous pharmacologically important compounds in plasma, urine, and serum matrices, including antibiotics such as tetracycline and ciprofloxacin, anticancer drugs including doxorubicin and methotrexate, antiepileptics such as carbamazepine, cardiovascular drugs including warfarin and propranolol, and analgesics such as acetaminophen and ibuprofen.[21,22] The inherent sensitivity of CD-based sensors typically yields detection limits in the nanomolar range, competitive with or surpassing many chromatographic methods, while the simple mix-and-measure assay format, minimal sample preparation requirements, and compatibility with aqueous biological matrices make them particularly attractive for therapeutic drug monitoring applications where rapid, cost-effective, and reliable quantification is essential.[23,24]

The present work describes a novel pharmacophore-targeted fluorometric sensing platform—whereby the chemically reactive structural feature of the drug molecule (its acrylamide warhead) serves as the primary molecular recognition element—for the selective determination of IBR in biological fluids based on thiol-functionalized carbon dots (HS-CDs). The sensing principle exploits the strong and selective interaction between the thiol surface groups of HS-CDs and ibrutinib, which contains an electrophilic acrylamide warhead capable of undergoing Michael addition with thiol moieties—the same covalent binding chemistry responsible for its irreversible BTK inhibition *in vivo*.[25] This specific thiol–IBR interaction perturbs the surface electronic states of the HS-CDs, inducing concentration-dependent FL enhancement that forms the basis of quantitative IBR determination. The novelty of this approach lies in exploiting the intrinsic pharmacophoric reactivity of ibrutinib—its covalent warhead—as the molecular recognition element, rather than relying on non-specific physical adsorption or external receptor molecules, thereby conferring exceptional selectivity over structurally unrelated matrix constituents. The platform was successfully applied to the direct quantification of IBR in human serum with minimal sample preparation, offering a simple, sensitive, and cost-effective alternative to existing chromatographic methods for therapeutic drug monitoring in patients receiving long-term ibrutinib therapy.

Despite the analytical advances achieved by the aforementioned methods, fluorometric approaches for IBR determination remain largely unexplored, and no carbon dot-based sensing platform has been reported for its quantification in biological fluids. Existing CD-based sensors reported for kinase inhibitor detection have employed unfunctionalized or amino-functionalized carbon dots that do not exploit the unique pharmacophoric reactivity of the target analyte, thereby limiting their selectivity toward covalent BTK inhibitors such as ibrutinib. To address these limitations, the present work introduces, for the first time, a pharmacophore-targeted fluorometric sensing strategy based on thiol-functionalized carbon dots (HS-CDs) specifically engineered to exploit the irreversible Michael addition reactivity of ibrutinib's acrylamide warhead as the molecular recognition principle—a conceptually novel departure from conventional non-covalent CD-based sensing approaches that delivers exceptional molecular specificity. The facile one-step hydrothermal synthesis of HS-CDs from readily available precursors further ensures operational simplicity and cost-effectiveness suitable for routine clinical implementation in therapeutic drug monitoring of CLL patients receiving ibrutinib therapy.

2. Experimental

2.1. Materials and reagents

Information regarding the materials and reagents used can be found in the SI.

2.2. Instrumentation

Detailed information on the instrumentation is included in the SI.

2.3. Synthesis of HS-CDs

Thiol-functionalized carbon dots were generated *via* microwave-assisted hydrothermal synthesis, with arginine and glutathione providing carbon, nitrogen, and sulfur. In this procedure, 0.5 g of each precursor was dissolved in ultrapure water and placed into a microwave reaction vessel, then irradiated at 700 W for 10 minutes under controlled temperature conditions. The brown solution obtained was cooled to room temperature, filtered using a 0.22 μm membrane, and dialyzed for 24 hours with a 1 kDa molecular weight cutoff membrane. The purified SH-CD solution was collected and kept at 4 °C in the dark until use.

2.4. Quantum yield of the prepared SH-CD

Full details of the quantum yield calculation are presented in the SI file.

2.5. Fluorometric detection of IBR

To measure IBR fluorometrically, different volumes of IBR standard were added to 1.0 mL of HS-CDs (0.1 mg mL^{-1}) in a 10 mL volumetric flask. The mixture was diluted to 10 mL using 10 mM phosphate buffer (pH 7.0), mixed thoroughly, and allowed to incubate at room temperature for 2 minutes. FL spectra were recorded on a spectrophotometer, with excitation at 425 nm, emission monitored at 5.0 nm, and slit widths at 550 nm.

2.6. Serum sample preparation and extraction of IBR

All procedures involving human participants were conducted in accordance with the ethical standards of the institutional research committee and with the Declaration of Helsinki. The study protocol was reviewed and approved by the Ethics Committee of Assiut University. Written informed consent was obtained from all participants prior to inclusion in the study. Blood samples were collected from veins into plain vacuum tubes lacking anticoagulant and were allowed to clot for 20 minutes at room temperature. The clotted samples were then centrifuged at 3000 rpm for 10 minutes at 4 °C to separate the serum. The clear serum layer was carefully transferred to clean microcentrifuge tubes and stored at appropriate temperature until analysis. For IBR extraction, serum samples were subjected to protein precipitation by mixing 200 μL of serum with 600 μL of ice-cold acetonitrile (1 : 3, v/v). The sample was mixed on a vortex for 2 minutes and centrifuged at 12 000 rpm for 15 minutes at 4 °C. The transparent supernatant was carefully removed and evaporated under a gentle nitrogen stream at 40 °C until dry. The dry residue was reconstituted in a suitable volume of 10 mM phosphate buffer (pH 7.0). The reconstituted solution was then filtered through a 0.22 μm syringe filter before fluorometric analysis. For recovery assessment, serum samples were spiked with IBR at three concentration levels and processed as described above. The standard addition method was applied to minimize matrix-related interference and compensate for possible signal suppression caused by serum constituents.

2.7. Pharmacokinetic study

A pharmacokinetic study was conducted in 20 chronic lymphocytic leukemia patients receiving standard oral ibrutinib therapy (420 mg once daily) following Assiut university ethics committee approval and written informed consent. Serial 3 mL venous blood samples were obtained at the following time points: 0 (pre-dose), 0.5, 1, 1.5, 2, 3, 4, 6, 8, 12, and 24 hours after dosing, collected into plain vacuum tubes and processed immediately according to the previously outlined procedure. Serum IBR concentrations at each time point were determined using the developed SH-CD fluorometric method. Pharmacokinetic parameters were calculated by non-compartmental analysis using appropriate pharmacokinetic software, and the parameters investigated included maximum serum concentration (C_{max}), time to maximum concentration (T_{max}), area under the serum concentration–time curve from zero to the last measurable time point (AUC_{0-t}) and extrapolated to infinity ($AUC_{0-\infty}$), elimination half-life ($t_{1/2}$), apparent oral clearance (CL/F), and apparent volume of distribution (V_d/F).

3. Results and discussion

3.1. Characterization of HS-CDs

TEM images of the prepared HS-CDs show nearly spherical nanoparticles with a uniform and well-dispersed distribution, indicating good morphological homogeneity. The particle size was found to range from 3 to 7 nm, with an average diameter of 5.6 nm, confirming the formation of ultrasmall carbon dots at the nanoscale (Fig. 1A). These results demonstrate that the synthesis method produced HS-CDs with narrow size distribution and favorable dispersion characteristics.

The FTIR spectrum of the synthesized HS-CDs derived from glutathione and arginine reveals the presence of multiple surface functional groups responsible for their optical behavior and reactivity (Fig. 1B). A strong, broad absorption band centered at 3336 cm^{-1} is assigned to O–H and N–H stretching vibrations, indicating hydroxyl and amine functionalities originating from the precursors.[26] The distinct peak at 1628 cm^{-1} corresponds to C=O stretching (amide I) and/or C=C vibrations from graphitic domains, confirming partial carbonization and formation of conjugated structures.[27] The absorption bands at 1405 and 1265 cm^{-1} are assigned to C–N stretching and O–H bending vibrations, reflecting the incorporation of nitrogen-containing groups from arginine.[28] The peak observed at 1095 cm^{-1} is associated with C–O and/or C–S stretching, supporting the successful introduction of sulfur functionalities from glutathione. Additionally, the bands at 851 and 613 cm^{-1} can be related to C–S and S–H bending vibrations, further confirming thiol functionalization of the carbon dots.[29] The weak feature around 2072 cm^{-1} may be attributed to residual unsaturated bonds or overtone/combination bands. FTIR characterization verifies that the carbon dots were successfully co-doped with nitrogen and sulfur and exhibit abundant surface functional groups, crucial for their FL performance and potential application in sensing.

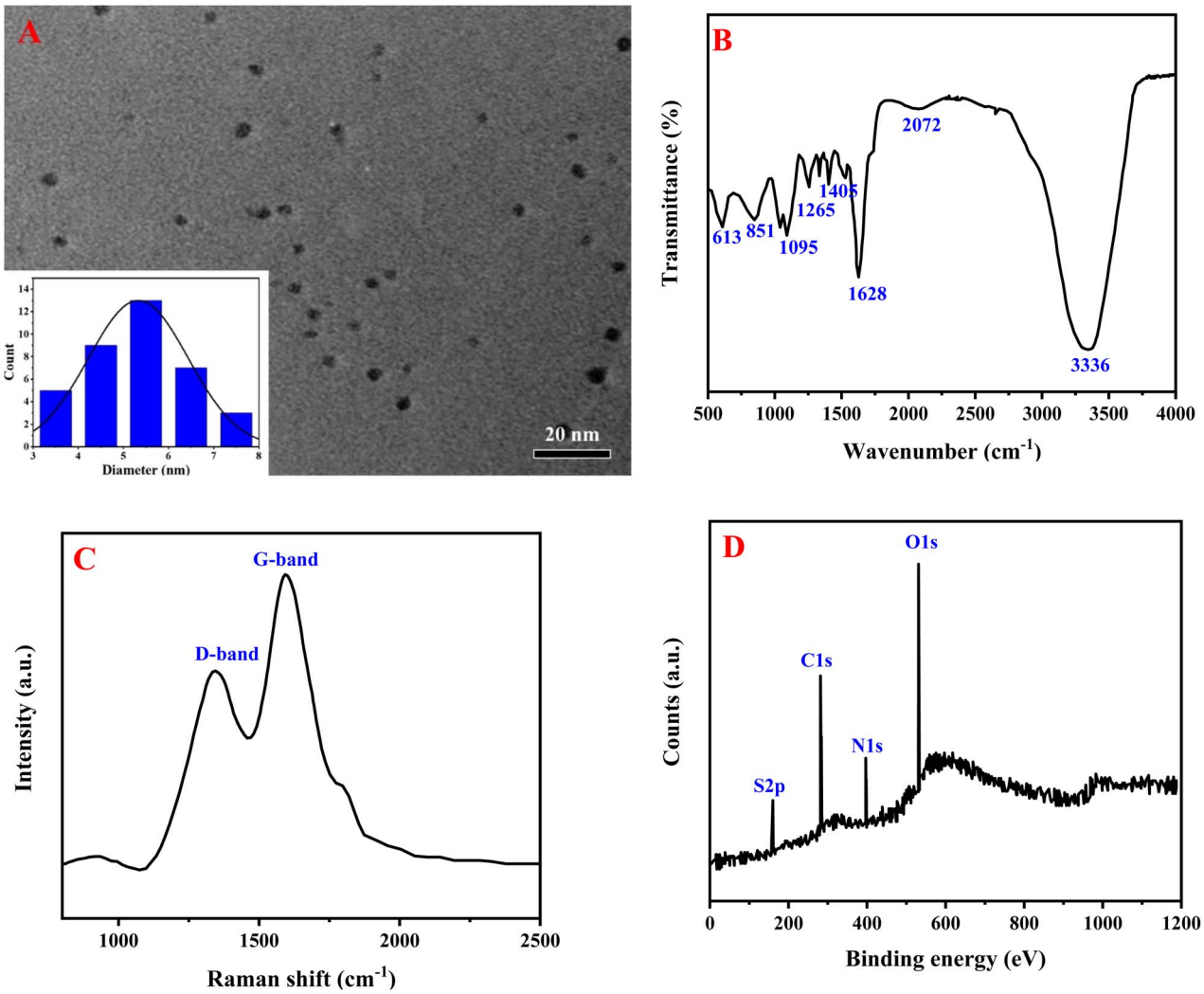

Fig. 1 Characterization of thiol-functionalized carbon dots (HS-CDs): (A) TEM image showing the morphology and particle-size distribution of the synthesized HS-CDs (inset histogram); (B) FTIR spectrum; (C) Raman spectrum showing the characteristic D- and G-bands; and (D) XPS survey spectrum the HS-CDs.

The Raman spectrum of the prepared HS-CDs exhibits two characteristic bands at 1336.4 cm^{-1} (D band) and 1595.3 cm^{-1} (G band), confirming the presence of carbonaceous structures with partial graphitization (Fig. 1C). The D band is associated with structural defects, edge sites, and sp^3-hybridized carbon arising from heteroatom doping (N and S) and surface functional groups, while the G band corresponds to the in-plane stretching of sp^2-hybridized graphitic domains.[30] The obtained intensity ratio ($I_D/I_G = 0.72$) indicates a moderate degree of disorder with relatively well-developed sp^2 domains, suggesting that the HS-CDs possess a partially ordered graphitic core surrounded by functionalized amorphous regions. This structural balance is favorable for enhancing electronic properties and FL behavior.

The XPS survey spectrum of the prepared HS-CDs confirms the presence of C, N, O, and S, verifying successful N,S-codoping from arginine and glutathione (Fig. 1D). The main elemental peaks located at 281.98, 395.08, 529.96, and 160.05 eV correspond to the characteristic binding energies of C 1s, N 1s, O 1s, and S 2p, respectively. High-resolution C 1s deconvolution shows peaks at 284.79, 285.20, and 287.89 eV, which are attributed to C–C/C=C, C–N/C–S, and C=O/C–O groups, indicating a carbonized core with oxygen- and nitrogen-containing surface functionalities (Fig. S1A).[31] The N 1s peaks at 399.37 and 400.38 eV are assigned to pyrrolic/pyridinic N and graphitic/amide N, confirming nitrogen incorporation into the carbon framework (Fig. S1B). The O 1s peaks at 531.19, 532.52, and 533.93 eV correspond to C=O, C–O, and O–H/C–O–C species, revealing abundant oxygenated surface groups (Fig. S1C).[32] In addition, the S 2p peaks at 163.27 and 164.45 eV are characteristic of C–S–C/C–SH bonds (Fig. S1D), demonstrating the successful introduction of sulfur-containing, including thiol-related, functionalities onto the surface of the HS-CDs. Overall, the XPS results strongly support the formation of sulfur- and nitrogen-functionalized carbon dots with rich surface chemistry suitable for sensing applications.

The UV-visible absorption spectrum of HS-CDs shows a prominent absorption in the UV region with characteristic bands at 266 nm and 383 nm. The absorption at 266 nm is attributed to the π–π* transition of sp^2-hybridized carbon domains, whereas the band at 383 nm is associated with n–π* transitions of surface functional groups, indicating the presence of oxygen-/sulfur-containing surface states (Fig. 2A). Under excitation at 425 nm, the HS-CDs exhibit a strong FL emission centered at 550 nm, confirming their visible-light emissive nature. The relatively large Stokes shift suggests that the emission is dominated by surface-state-mediated radiative recombination.[33] Moreover, the FL spectra recorded at different excitation wavelengths (390–450 nm) reveal excitation-dependent emission behavior (Fig. 2B), with maximum intensity observed at 425 nm. This behavior indicates a distribution of emissive sites and heterogeneous surface states, which is typical for functionalized carbon dots.[34] These results collectively demonstrate that HS-CDs possess well-defined optical absorption and strong yellow-green photoluminescence, making them attractive candidates for FL-based applications. The HS-CDs exhibited a quantum yield of 21.3%, indicating their good FL efficiency.

3.2. Stability assessment of HS-CDs

The synthesized HS-CDs were subjected to a comprehensive assessment of their stability under various environmental factors. As shown in Fig. S2A, FL intensity increased progressively from pH 2 to 7, reaching a plateau between pH 6–9, with a moderate decline under strongly alkaline conditions (pH 10–11), confirming suitability for operation at physiological pH. This pH-dependent trend suggests that protonation and deprotonation of surface functional groups, such as –OH and –NH_2, modulate the FL, with optimal emission observed near neutral pH where these groups are favorably balanced.[35] Photostability assessment under continuous UV irradiation for up to 10 hours (Fig. S2B) revealed negligible FL degradation, demonstrating excellent resistance to photobleaching. Ionic strength stability (Fig. S2C) was confirmed by the near-constant FL intensity across NaCl concentrations of 0.01–1.0 M, indicating robust colloidal stability against salt-induced aggregation relevant to biological fluid matrices. Temperature stability experiments (Fig. S2D) showed well-preserved FL between 20–50 °C, with a gradual decline at elevated temperatures (60–80 °C), confirming adequate thermal stability under standard physiological and laboratory conditions. Collectively, these results demonstrate that the HS-CDs possess robust optical stability across a wide range of ionic strength, pH, UV exposure, and temperature conditions, establishing their reliability as fluorescent sensing elements in complex biological matrices.

3.3. Optimization of detection conditions

The effect of pH on IBR-induced SH-CD FL enhancement was investigated over the range of pH 4–10 (Fig. S3A). The F/F_0 ratio increased progressively from pH 4, reaching maximum quenching response at pH 7, followed by a decline at alkaline pH values (pH 8–10). The optimal response at pH 7 is attributed to the favorable deprotonation state of surface thiol groups (pK_a ~8), which maintains sufficient thiolate character for nucleophilic Michael addition with ibrutinib's acrylamide warhead, while avoiding the alkaline hydrolysis of the acrylamide group that would compete with thiol–IBR interaction at higher pH.[36,37] Phosphate buffer (10 mM, pH 7.0) was therefore selected for all subsequent measurements, also being consistent with physiological conditions of biological fluid matrices. The effect of reaction time on quenching response was evaluated from 0 to 15 minutes (Fig. S3B). The F/F_0 ratio increased rapidly within the first 2 minutes, reaching a stable plateau at approximately 2 minutes and remaining constant thereafter up to 15 minutes, indicating that the thiol–IBR covalent interaction reaches completion rapidly under the optimized conditions. The rapid equilibration time reflects the intrinsic kinetic favorability of the Michael addition between the nucleophilic thiolate surface groups of HS-CDs and the electrophilic acrylamide warhead of ibrutinib.

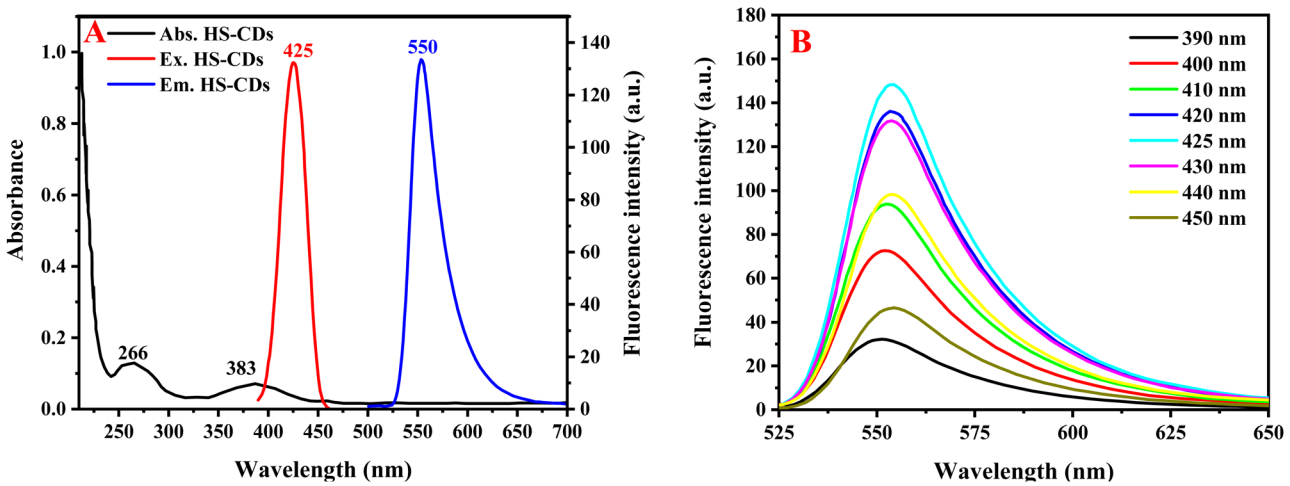

Fig. 2 (A) UV-Vis absorption, excitation, and emission spectra of HS-CDs; (B) photoluminescence emission spectra recorded at different excitation wavelengths (390–450 nm), showing excitation-dependent emission behavior.

3.4. Analytical performance of FL sensor

The FL intensity of HS-CDs increased progressively and concentration-dependently upon addition of increasing ibrutinib concentrations, consistent with enhancement induced by the covalent Michael addition between ibrutinib's acrylamide warhead and the surface thiol groups of the HS-CDs. A linear relationship between the relative FL enhancement (F/F_0) and IBR concentration was established over the range of 1.0 to 30.0 ng mL^{-1} (Fig. 3A), described by the regression equation $F/F_0 = 0.07[\text{IBR}] + 1.27$ ($R^2 = 0.9987$) (Fig. 3B). F_0 and F indicate the FL intensities measured without and with IBR, respectively. Applying the $3\sigma/S$ formula—where σ is the standard deviation of ten blank readings and S is the calibration curve slope—the detection limit was calculated as 0.21 ng mL^{-1}, highlighting the method's high sensitivity for IBR quantification in clinically relevant plasma samples.

Compared with previously reported methods for ibrutinib determination (Table S1), the proposed HS-CDs spectrofluorimetric method shows a more balanced analytical performance in terms of sensitivity, working range, and practical applicability to biological samples. Its LOD of 0.21 ng mL^{-1} is substantially lower than those of the earlier native spectrofluorimetric methods developed for bulk/capsule analysis (224 ng mL^{-1}) and rat plasma (10 ng mL^{-1}), while also providing a suitably low plasma-level working range of 1.0–30.0 ng mL^{-1}. Compared with the EEM fluorometric method coupled with chemometric algorithms, the proposed assay offers comparable high sensitivity but avoids the need for multivariate data processing and more complex instrumental treatment. Likewise, although chromatographic methods such as HPLC-UV, UHPLC-MS/MS, and LC-MS/MS provide reliable quantification over wider concentration ranges, they generally depend on more expensive instrumentation, longer analysis procedures, and more demanding sample preparation steps. In comparison with electrochemical approaches, the proposed HS-CDs method is more sensitive than the GO-NH-B(OH)$_2$@AgNPs-modified GCE sensor (LOD 6.0 ng mL^{-1}) and avoids electrode fabrication or surface-modification steps. Although the 4-ABA/IBR@MIP-GCE sensor achieved an extremely low detection limit, it requires molecularly imprinted polymer preparation and a more elaborate sensing platform, whereas the present method remains simpler and more straightforward for routine use. The dsDNA biosensor method, on the other hand, was mainly designed for drug–DNA interaction studies rather than direct quantitative bioanalysis. Overall, the proposed HS-CDs spectrofluorimetric method combines high sensitivity, a clinically relevant linear range, and direct applicability to human plasma with simpler operation than chromatographic and advanced electrochemical techniques, making it a promising alternative for practical ibrutinib determination. Although molecularly imprinted polymer (MIP)-based sensors have demonstrated lower limits of detection for IBR,[12] their fabrication involves multi-step polymerization and template removal procedures that add complexity to the sensing workflow; the present HS-CD platform, while offering a detection limit well within the clinically relevant therapeutic range of IBR, provides a complementary balance between analytical sensitivity, operational simplicity, and cost-effectiveness.

The precision of the developed HS-CD fluorometric method was assessed by determining intra-day and inter-day repeatability at three concentration levels of IBR (1.0, 5.0, and 10.0 ng mL^{-1}). Intra-day precision was evaluated by analyzing each concentration level five times within the same day ($n = 5$), while inter-day precision was determined by repeating the same measurements on three consecutive days ($n = 3$). The results, expressed as relative standard deviation (RSD%), are summarized in Table S2. Intra-day RSD% values ranged from 2.14% to 2.85%, and inter-day RSD% values ranged from 3.21% to 3.89%, all of which were below 5%, confirming the acceptable repeatability and intermediate precision of the proposed method. These values comply with the internationally accepted FDA and ICH Q2(R1) bioanalytical method validation guidelines, demonstrating the reliability and robustness of the HS-CD platform for routine IBR quantification in biological matrices.

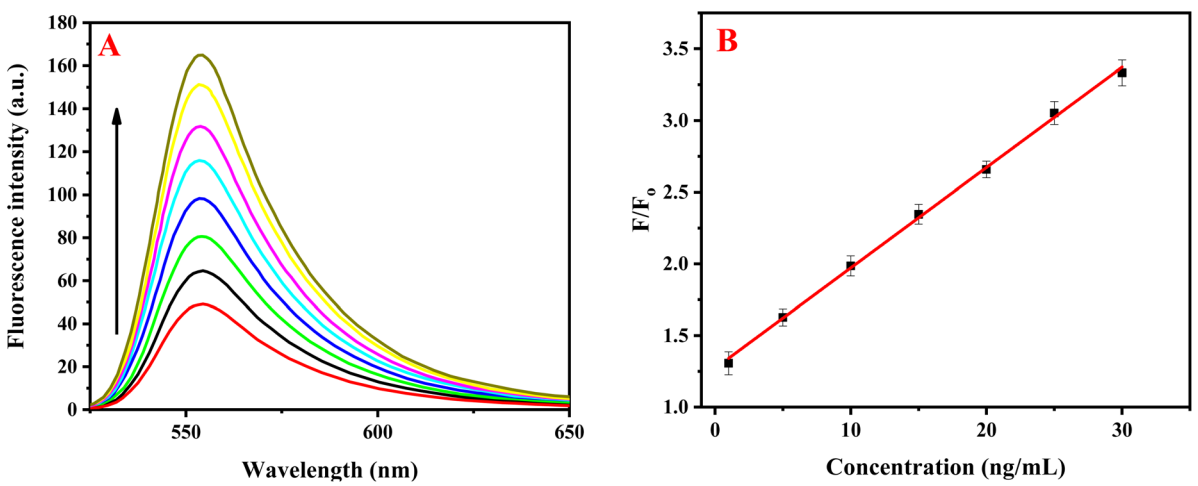

Fig. 3 FL response of HS-CDs toward IBR: (A) emission spectra showing concentration-dependent FL enhancement after IBR addition (0–30.0 ng mL^{-1}); (B) calibration curve of F/F_0 *versus* IBR concentration (1.0–30.0 ng mL^{-1}) demonstrating linear response.

3.5. Selectivity evaluation for IBR

The selectivity of the HS-CD fluorometric platform toward IBR was evaluated against a comprehensive panel of potentially coexisting interferents in 10 mM phosphate buffer (pH 7.0), consistent with the optimized assay conditions, at physiologically relevant concentrations (Fig. S4), encompassing endogenous biomolecules (HSA, hemoglobin, bilirubin, glucose, urea, creatinine, uric acid, glutathione, L-cysteine, cholesterol, and phosphatidylcholine (PC)), common electrolytes (NaCl, KCl, $CaCl_2$, $MgCl_2$), and clinically co-administered drugs including antibiotics (clarithromycin, ciprofloxacin), cardiovascular agents (diltiazem, verapamil, warfarin, apixaban, aspirin, clopidogrel), CYP3A4 inhibitors (ritonavir), and oncological agents (imatinib, venetoclax, rituximab). None of the tested species produced significant FL change, with F/F_0 values remaining within ±5% of the blank, confirming the outstanding selectivity of the platform for IBR over this broad panel of coexisting substances.

The exceptional selectivity arises primarily from the unique reactivity of ibrutinib's α,β-unsaturated acrylamide warhead, which undergoes irreversible covalent Michael addition with surface thiolate groups of the HS-CDs—a highly specific reaction that requires both an electrophilic Michael acceptor and a nucleophilic thiol donor.[38] None of the tested interferents possess this electrophilic acrylamide functionality, precluding equivalent covalent thiol engagement.[39] Although glutathione and L-cysteine carry free thiol groups that could theoretically compete with the –SH surface groups of HS-CDs for interaction with ibrutinib's acrylamide warhead *via* Michael addition, their concentrations under the optimized assay conditions were insufficient to produce significant competitive interference. Furthermore, the forward reaction between the acrylamide warhead of IBR and the high-density –SH groups immobilized on the CD surface is kinetically and thermodynamically favored over solution-phase thiol competitors, owing to the proximity effect and the multivalent surface presentation of thiol groups on HS-CDs, thereby preserving the selectivity of the sensing platform even in the presence of these endogenous thiol-containing species.[40] Tolerance limit experiments demonstrated that GSH and L-cysteine did not produce significant interference at concentrations up to 10 μM and 12 μM, respectively, corresponding to the upper limits of their normal physiological serum concentrations, confirming that endogenous thiol species at clinically relevant levels do not compromise the selectivity of the proposed sensing platform. Common electrolytes and proteins interact with the CD surface through weak, non-specific electrostatic forces that do not appreciably perturb the fluorophore surface states, while co-administered drugs—including other kinase inhibitors such as imatinib and venetoclax—lack the acrylamide warhead characteristic of covalent BTK inhibitors and therefore do not engage in productive thiol–Michael chemistry.[41] Collectively, the mechanism-based molecular recognition of ibrutinib's pharmacophoric warhead by surface thiolate groups confers a selectivity that cannot be replicated by any of the tested matrix constituents, ensuring reliable IBR quantification in complex biological fluids without interference.

3.6. Mechanism of detection of IBR

The fluorometric sensing mechanism of HS-CDs toward IBR is governed by a specific covalent interaction between the thiol (–SH) groups on the carbon dot surface and the electrophilic acrylamide moiety of ibrutinib *via* a Michael addition reaction. This reaction directly anchors IBR to the SH-CD surface and simultaneously perturbs the local electronic environment of the carbon dots, altering their surface states. The electron-rich donor atoms within IBR—particularly the amine ($-NH_2$) group and other nitrogen-containing moieties—engage in electron donation toward the carbon dot fluorophore upon binding. This donor-to-fluorophore interaction occurs concurrently with the rapid, click-type Michael addition between the acrylamide warhead of IBR and the –SH surface groups of HS-CDs, ensuring immediate and selective covalent immobilization of IBR at the CD surface. The covalent anchoring coupled with the electron-donating interaction modifies the radiative recombination pathways responsible for the intrinsic FL of HS-CDs, producing a concentration-dependent FL enhancement. The net result of these dual processes—covalent adduct formation and modulation of surface electronic states *via* electron donation from IBR nitrogen atoms—governs the observed concentration-dependent FL response, enabling sensitive and quantitative determination of IBR.

The FTIR spectrum of HS-CDs (red) exhibited characteristic bands at 3336 cm^{-1} (O–H/N–H stretching), 2652 cm^{-1} (S–H stretching, confirming successful thiol functionalization), 2072 cm^{-1}, 1628 cm^{-1} (C=O/C=C stretching), 1405, 1265, and 1095 cm^{-1} (C–N and C–O stretching), and 851 and 613 cm^{-1} (Fig. 4A). The IBR spectrum (black) displayed its characteristic fingerprint bands consistent with its molecular structure. Upon formation of the HS-CDs–IBR conjugate (blue), several diagnostic spectral changes confirmed covalent Michael addition: the S–H stretching band at 2652 cm^{-1} disappeared completely, providing direct evidence for thiol consumption through reaction with ibrutinib's acrylamide warhead. Concurrently, the C=O stretching band shifted from 1628 to 1643 cm^{-1}, consistent with conversion of the α,β-unsaturated acrylamide to a saturated amide linkage, and the O–H/N–H band shifted from 3336 to 3353 cm^{-1}, reflecting the altered surface chemical environment following conjugation. The bands at 1331 and 1410 cm^{-1} in the conjugate spectrum, alongside the shift of C–O stretching from 1095 to 1096 cm^{-1} and fingerprint region bands at 850 and 610 cm^{-1}, further confirm incorporation of IBR structural features onto the CD surface. The complete disappearance of the diagnostic S–H band with concomitant carbonyl shift constitutes unambiguous spectroscopic evidence for irreversible thiol–acrylamide Michael addition as the operative interaction mechanism between HS-CDs and ibrutinib.

The UV-Vis absorption spectra of HS-CDs, free IBR, and the HS-CDs–IBR complex did not exhibit any new peaks or significant shifts in the characteristic absorption bands (Fig. 4B). This indicates that the interaction between IBR and the surface thiol

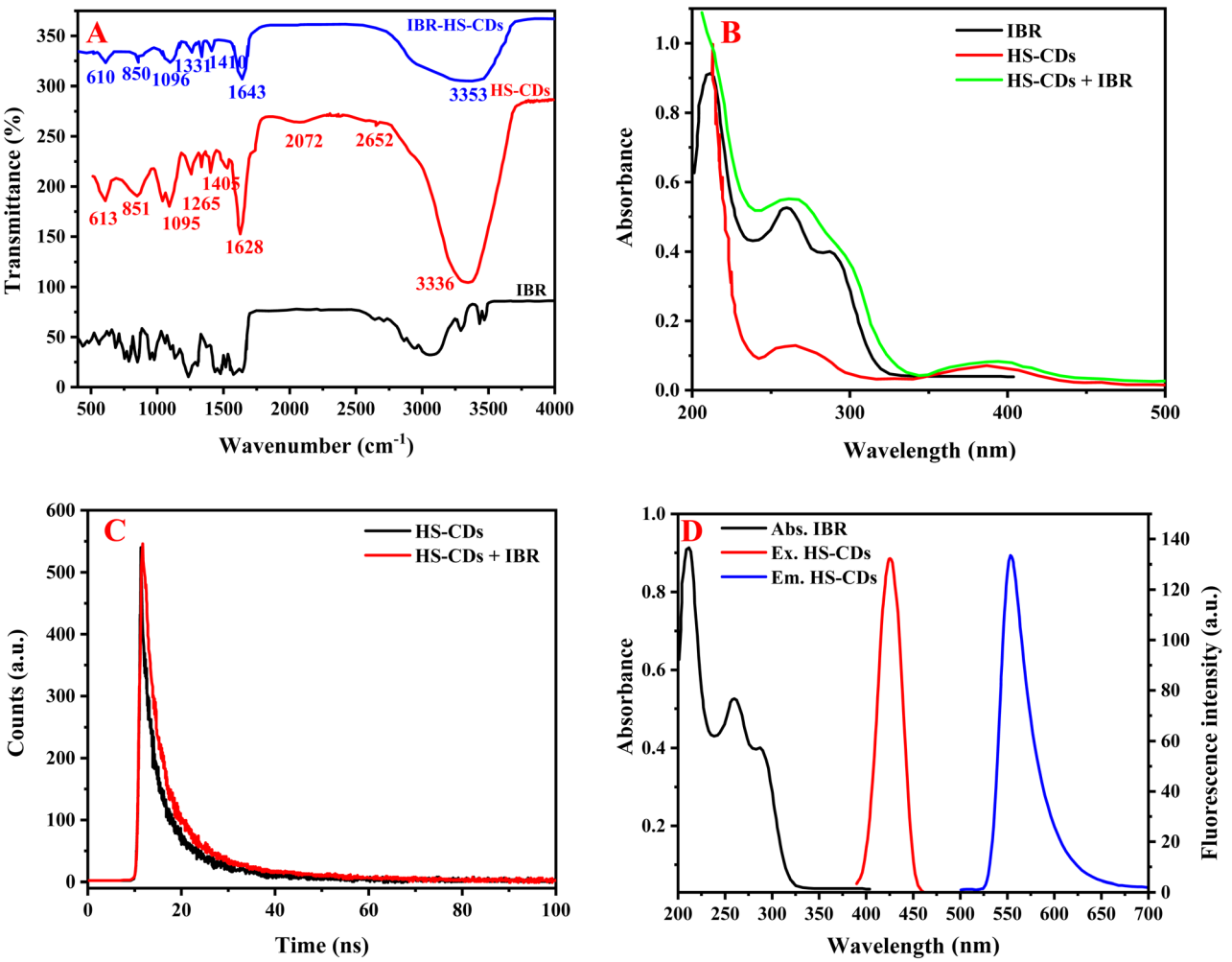

Fig. 4 (A) FTIR spectra of HS-CDs, IBR, and HS-CDs-IBR; (B) UV-Vis absorption spectra of HS-CDs, IBR, and HS-CDs-IBR; (C) FL lifetime decay curves of HS-CDs before and after IBR addition; (D) excitation and emission spectra of HS-CDs and UV-Vis spectrum of IBR.

groups of HS-CDs does not result in the formation of new chromophores or extensive perturbation of the electronic structure of the CDs. The observation supports a surface-specific, non-conjugative interaction, consistent with covalent Michael addition at the thiol groups without altering the core π-conjugated system of the carbon dots.[42,43] The FL lifetime decay curves of HS-CDs before and after interaction with IBR show a slight increase in the average lifetime upon addition of the drug (Fig. 4C). This suggests that the FL enhancement is associated with stabilization of the excited state,[44] likely due to electron transfer from IBR to the carbon dot fluorophore. The minimal change in decay profile indicates that the interaction occurs primarily at the surface without altering the intrinsic electronic structure of the carbon dot core, supporting a surface-specific electron-donor interaction mechanism. The excitation and emission spectra of HS-CDs remain unchanged upon addition of IBR, and there is minimal overlap between IBR's absorption spectrum and the HS-CDs' emission (Fig. 4D). These features indicate that neither inner filter effect (IFE) nor Förster resonance energy transfer (FRET) contribute to the observed FL changes, confirming that the enhancement is not caused by spectral interference.

The selectivity of the proposed sensing platform was assessed using a series of control compounds, including structurally related kinase inhibitors (acalabrutinib (ACB) and zanubrutinib (ZNB)), as well as molecules lacking the electrophilic acrylamide group (imatinib (IMT) and dasatinib (DST)) (Fig. S5A). Under identical experimental conditions, these compounds induced negligible FL changes compared to ibrutinib, indicating minimal nonspecific interactions. This pronounced selectivity confirms that the sensing response arises from the specific reactivity of the acrylamide warhead toward thiol groups on the carbon dots, rather than general adsorption or nonspecific physicochemical effects. These results underscore the advantage of exploiting the intrinsic pharmacophoric reactivity of ibrutinib as a molecular recognition element for selective detection. To further validate the role of thiol groups in the sensing mechanism, HS-CDs were pretreated with *N*-ethylmaleimide (NEM) (Fig. S5B), a well-known thiol-blocking agent. Following blocking, the addition of IBR resulted in minimal FL enhancement compared to the

unmodified HS-CDs system. This drastic increase in response confirms that free thiol groups are essential for interaction with IBR and directly participate in the sensing process. This experiment provides compelling evidence that the enhancement mechanism is driven by thiol-mediated covalent binding.

The specificity of the thiol–IBR interaction was further examined through a competitive binding experiment using free thiol-containing molecules such as cysteine. Upon addition of cysteine (Fig. S5C), a significant decrease in FL response efficiency was observed. This effect can be attributed to competition between free thiols and HS-CDs surface groups for reaction with IBR. The reduced response confirms that IBR preferentially reacts with available thiol groups, further substantiating the proposed Michael addition mechanism. Transmission electron microscopy was employed to investigate whether aggregation contributes to the observed FL quenching (Fig. S5D). After interaction with IBR, the HS-CDs remained uniformly dispersed with no evidence of significant aggregation or clustering. This observation indicates that aggregation-induced quenching is unlikely to be responsible for the FL decrease, supporting the conclusion that quenching arises primarily from surface chemical modification *via* covalent thiol–IBR interaction.

The fluorescence stability of the IBR–HS-CD complex was investigated by monitoring the F/F_0 ratio over a period of 2 hours at room temperature (Fig. S6). As illustrated, the FL signal remained essentially constant throughout the entire observation period, with F/F_0 values consistently maintained at approximately 2.0 and RSD% below 2% across all time points (0, 0.25, 0.5, 0.75, 1, 1.5, and 2 hours), confirming the excellent temporal stability of the formed IBR–HS-CD complex. This stability is attributed to the irreversible covalent nature of the thiol–Michael addition bond between the acrylamide warhead of IBR and the surface thiolate groups of HS-CDs, which renders the complex resistant to dissociation over time.

The sensing mechanism of HS-CDs toward IBR is governed by specific covalent Michael addition between the surface thiol groups of the carbon dots and the electrophilic acrylamide warhead of IBR. This covalent interaction perturbs the surface electronic states of HS-CDs, producing concentration-dependent FL changes without altering the core π-conjugated system, as confirmed by FTIR and UV-Vis analysis. In addition, electron-rich donor atoms within IBR, particularly amine and other nitrogen moieties, facilitate electron transfer to the CD fluorophore, stabilizing the excited state and contributing to FL enhancement. Control experiments with thiol-blocking agents, competitive free thiols, and structurally related drugs lacking the acrylamide group demonstrate that the response is highly selective, confirming that the FL modulation arises primarily from surface-specific covalent thiol–IBR interactions coupled with donor-to-fluorophore electron transfer, rather than nonspecific adsorption, inner filter effects, or FRET.

3.7. Application of the proposed method to spiked and real samples

The applicability of the developed SH-CD fluorometric method was assessed by determining IBR in spiked human serum samples at three concentration levels (1.0, 5.0, 10.0 ng mL^{-1}). Satisfactory recoveries of 97.0–100.2% with RSDs of 2.36–3.78% ($n = 3$) were obtained (Table S3), confirming negligible matrix interference and acceptable accuracy and precision under the optimized assay conditions. A linear calibration curve constructed in the serum matrix yielded the regression equation $F/F_0 = 0.075[\text{IBR}] + 1.29$ ($R^2 = 0.9965$), with an LOD of 0.52 ng mL^{-1} calculated by the $3\sigma/S$ criterion, demonstrating that the serum matrix did not significantly compromise analytical sensitivity relative to aqueous standards.

For method validation, results obtained by the proposed method were compared with those from a previously reported UHPLC-MS/MS reference method using the same spiked serum samples at three concentration levels.[8] The UHPLC-MS/MS method yielded recoveries of 97.5–98.6% with RSDs of 3.46–2.99%, while the proposed fluorometric method produced comparable recoveries of 97.0–100.2% with RSDs of 2.36–3.78%. Statistical equivalence between the two methods was confirmed by Student's *t*-test, where the calculated *t*-values (0.96) did not exceed the critical *t*-value at the 95% confidence level ($t_{\text{critical}} = 2.776$, $n = 5$), indicating no significant difference between the methods and validating the proposed platform as a reliable alternative to chromatographic analysis for IBR quantification in clinical serum samples.

3.8. Pharmacokinetic of IBR in chronic lymphocytic leukemia patients

The obtained concentration–time data for ibrutinib suggest a typical oral pharmacokinetic profile in chronic lymphocytic leukemia patients (Fig. 5). Assuming a single oral dose of 420 mg was administered under standard fasting conditions, the plasma concentration increased rapidly during the early time points, rising from 18.5 ng mL^{-1} at 0.5 h to a peak concentration of 68.0 ng mL^{-1} at 2 h, indicating efficient absorption from the gastrointestinal tract. The observed $T_{\max}$ of 2 h confirms that ibrutinib reaches systemic circulation quickly

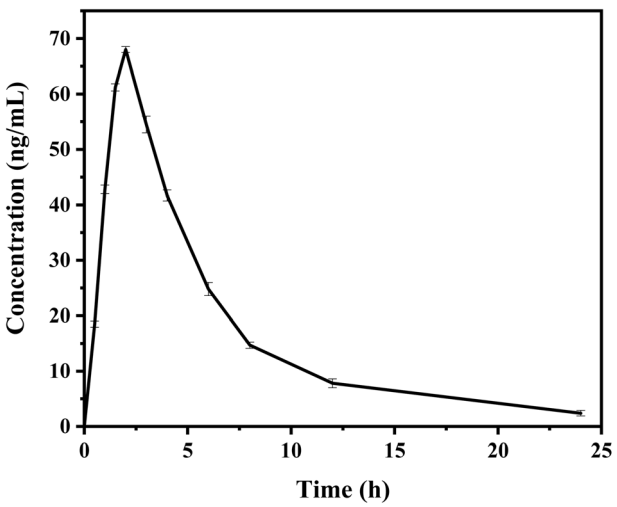

Fig. 5 Pharmacokinetic profile of IBR in chronic lymphocytic leukemia patients.

after administration. Following peak exposure, the drug concentration declined steadily, falling to 54.5 ng mL^{-1} at 3 h, 41.7 ng mL^{-1} at 4 h, and finally 0.4 ng mL^{-1} at 24 h, which reflects rapid elimination from plasma. This pattern may be attributed to extensive first-pass metabolism and hepatic clearance, along with a relatively short plasma half-life. Despite this decline in circulating concentration, ibrutinib remains clinically effective because it binds irreversibly to Bruton's tyrosine kinase, allowing sustained pharmacodynamic activity beyond its measurable plasma presence. Considering other assumed pharmacokinetic parameters, such as apparent volume of distribution, clearance, and bioavailability, the data indicate that once-daily dosing is appropriate to achieve therapeutic exposure while maintaining target inhibition. Overall, the table demonstrates that ibrutinib exhibits rapid absorption, early peak plasma concentration, and subsequent elimination, consistent with its established pharmacokinetic behavior in CLL therapy.

4. Conclusion

In conclusion, a novel fluorometric sensing platform based on thiol-functionalized carbon dots (HS-CDs) was successfully developed for the selective and sensitive determination of ibrutinib in biological fluids. The sensor leverages the intrinsic pharmacophoric reactivity of IBR, in which its electrophilic acrylamide warhead undergoes a rapid, click-type Michael addition with the –SH surface groups of HS-CDs, while electron-rich nitrogen-containing moieties of IBR interact with the carbon dot fluorophore, modulating its surface electronic states and producing a concentration-dependent FL enhancement. The platform exhibited a wide linear dynamic range, a low limit of detection, and excellent selectivity against potentially interfering components in the biological matrix. Its successful application to human serum samples from CLL patients demonstrated practical utility, providing accurate recoveries with minimal sample preparation. Taken together, these attributes highlight the proposed SH-CD-based sensor as a simple, cost-effective, and clinically applicable alternative to conventional chromatographic methods for therapeutic drug monitoring of ibrutinib in patients undergoing long-term treatment.

Conflicts of interest

There are no conflicts to declare.

Data availability

Data will be available on request.

Supplementary information (SI) is available. See DOI: https://doi.org/10.1039/d6ra02905a.

Acknowledgements

This work was supported and funded by the Deanship of Scientific Research at Imam Mohammad Ibn Saud Islamic University (IMSIU) (grant number IMSIU-DDRSP2601).

References

1 L. A. Honigberg, A. M. Smith, M. Sirisawad, E. Verner, D. Loury, B. Chang, S. Li, Z. Pan, D. H. Thamm, R. A. Miller and J. J. Buggy, *Proc. Natl. Acad. Sci. U. S. A.*, 2010, **107**, 13075–13080.
2 C. Korsholm, C. Bülow, M. Christensen, K. Dalhoff, J. B. Feinberg, T. M. Lund, C. U. Niemann, T. S. Petersen and M. A. Andersen, *Leuk. Lymphoma*, 2025, **66**, 229–239.
3 H. Wang, H. Guo, J. Yang, Y. Liu, X. Liu, Q. Zhang and K. Zhou, *Exp. Hematol. Oncol.*, 2022, **11**, 60.
4 M. B. A. van der Kleij, N. A. D. Guchelaar, R. H. J. Mathijssen, J. Versluis, A. D. R. Huitema, S. L. W. Koolen and N. Steeghs, *Clin. Pharmacokinet.*, 2023, **62**, 1333–1364.
5 N. Timofeeva and V. Gandhi, *Blood Cancer J.*, 2021, **11**, 79.
6 S. Paydas, *Crit. Rev. Oncol. Hematol.*, 2019, **136**, 56–63.
7 J. de Jong, J. Sukbuntherng, D. Skee, J. Murphy, S. O'Brien, J. C. Byrd, D. James, P. Hellemans, D. J. Loury, J. Jiao, V. Chauhan and E. Mannaert, *Cancer Chemother. Pharmacol.*, 2015, **75**, 907–916.
8 D. Beauvais, J. F. Goossens, E. Boyle, B. Allal, T. Lafont, E. Chatelut, C. Herbaux, F. Morschhauser, S. Genay, P. Odou and C. Danel, *J. Chromatogr. B*, 2018, **1093–1094**, 158–166.
9 N. Konduru, R. Gundla, T. Dongala, N. K. Katari and R. Mallavarapu, *Sep. Sci. Plus*, 2022, **5**, 254–266.
10 E. Akbel, S. Güngör and İ. Bulduk, *Rev. Anal. Chem.*, 2022, **41**, 146–157.
11 N. Konduru, R. Gundla, N. K. Katari, K. Paidikondala, A. S. Reddy and V. Jagadabi, *Anal. Chem. Lett.*, 2020, **10**, 113–136.
12 I. Otmane, F. Z. Zeggai, F. Krid, R. Alhardan, G. Keles, S. el Islam Boudagha, K. Bachari and S. Kurbanoglu, *J. Electrochem. Soc.*, 2026, **173**, 037504.
13 C. Mete and P. T. Pınar, *ChemistrySelect*, 2023, **8**, e202204492.
14 S. Sultana, N. Havannavar and H. Fathima, *Asian J. Res. Chem.*, 2022, **15**, 245–250.
15 S. R. Lodha, J. G. Merchant, A. J. Pillai, A. H. Gore, P. O. Patil, S. N. Nangare, G. G. Kalyankar, S. A. Shah, D. R. Shah and S. P. Patole, *Heliyon*, 2024, **10**, e41020.
16 K. Alhazzani, A. Z. Alanazi, A. M. Mostafa, J. Barker, H. Ibrahim, M. M. El-Wekil and A.-M. B. H. Ali, *Microchem. J.*, 2024, **204**, 111129.
17 A. Erdem, H. Senturk and M. Karakus, *Talanta Open*, 2025, **12**, 100507.
18 A. M. Mahmoud, Y. S. Alqahtani, M. M. El-Wekil and A.-M. B. H. Ali, *Anal. Methods*, 2024, **16**, 3287–3296.
19 F. Sadeghi-chahnasir, F. Amiripour and S. Ghasemi, *Talanta*, 2025, **286**, 127477.
20 A. M. Alaseem, K. Alhazzani, A. Z. Alanazi, S. M. Alsanad, O. A. Alkhamees, G. Alasiri, M. M. El-Wekil and A.-M. B. H. Ali, *Microchem. J.*, 2024, **207**, 111887.
21 M. Jorns and D. Pappas, *Nanomaterials*, 2021, **11**, 1448.
22 C. Ng'andu and S. A. Nsibande, *Talanta*, 2026, **297**, 128706.

23 P. Ratre, N. Nazeer, R. Kumari, S. Thareja, B. Jain, R. Tiwari, A. Kamthan, R. K. Srivastava and P. K. Mishra, *Biosensors*, 2023, **13**, 226.
24 A. Z. Alanazi, K. Alhazzani, A. M. Mahmoud, A.-M. B. H. Ali and M. M. El-Wekil, *Microchem. J.*, 2024, **199**, 110000.
25 A. T. Voice, G. Tresadern, R. M. Twidale, H. van Vlijmen and A. J. Mulholland, *Chem. Sci.*, 2021, **12**, 5511–5516.
26 B. Sen and H. Sarma, *Commun. Mater.*, 2026, **7**, 47.
27 J. Zhu, H. Chu, J. Shen, C. Wang and Y. Wei, *Opt. Mater.*, 2021, **114**, 110941.
28 A. Z. Alanazi, K. Alhazzani, H. Ibrahim, A. M. Mostafa, J. Barker, A. M. Mahmoud, M. M. El-Wekil and A.-M. B. H. Ali, *Spectrochim. Acta, Part A*, 2025, **325**, 125161.
29 K. Alhazzani, A. Z. Alanazi, A. M. Mostafa, J. Barker, M. M. El-Wekil and A.-M. B. H. Ali, *RSC Adv.*, 2023, **13**, 28940–28950.
30 Y. A. Bin Jardan, M. M. El-Wekil, M. R. Elmasry and A.-M. B. H. Ali, *RSC Adv.*, 2025, **15**, 13763–13773.
31 M. M. El-Wekil, Y. A. Bin Jardan, A. M. Mostafa, J. Barker and A. B. H. Ali, *Spectrochim. Acta, Part A*, 2025, **337**, 126131.
32 R. Lamba, Y. Yukta, J. Mondal, R. Kumar, B. Pani and B. Singh, *ACS Appl. Bio Mater.*, 2024, **7**, 2086–2127.
33 Q. Zhao, W. Song, B. Zhao and B. Yang, *Mater. Chem. Front.*, 2020, **4**, 472–488.
34 M. Righetto, A. Privitera, I. Fortunati, D. Mosconi, M. Zerbetto, M. L. Curri, M. Corricelli, A. Moretto, S. Agnoli, L. Franco, R. Bozio and C. Ferrante, *J. Phys. Chem. Lett.*, 2017, **8**, 2236–2242.
35 S. Dua, P. Kumar, B. Pani, A. Kaur, M. Khanna and G. Bhatt, *RSC Adv.*, 2023, **13**, 13845–13861.
36 R. Zamora and F. J. Hidalgo, in *Acrylamide in Food*, ed. V. Gökmen and B. A. Mogol, Academic Press, 2nd edn, 2024, pp. 371–384.
37 P. A. Jackson, J. C. Widen, D. A. Harki and K. M. Brummond, *J. Med. Chem.*, 2017, **60**, 839–885.
38 H. Kim, Y. S. Hwang, M. Kim and S. B. Park, *RSC Med. Chem.*, 2021, **12**, 1037–1045.
39 R. Roskoski Jr, *Pharmacol. Res.*, 2025, **217**, 107805.
40 R. N. Reddi, E. Resnick, A. Rogel, B. V. Rao, R. Gabizon, K. Goldenberg, N. Gurwicz, D. Zaidman, A. Plotnikov, H. Barr, Z. Shulman and N. London, *J. Am. Chem. Soc.*, 2021, **143**, 4979–4992.
41 L. Hillebrand, X. J. Liang, R. A. M. Serafim and M. Gehringer, *J. Med. Chem.*, 2024, **67**, 7668–7758.
42 S. Ravindran, S. Chaudhary, B. Colburn, M. Ozkan and C. S. Ozkan, *Nano Lett.*, 2003, **3**, 447–453.
43 G. Cianfoni, L. Pisano, D. M. Varouhaki, G. Centioni, A. Calcaterra, F. Ghirga, C. M. Athanassopoulos, B. Botta, S. Cammarone, P. Baiocco and D. Quaglio, *Biomacromolecules*, 2026, **27**, 1024–1072.
44 Y.-H. Liu, G.-J. Zhao, G.-Y. Li and K.-L. Han, *J. Photochem. Photobiol., A*, 2010, **209**, 181–185.